Hindawi
Shock and Vibration
Volume 2018, Article ID 7987502, 16 pages
https://doi.org/10.1155/2018/7987502

Research Article

Optimal Design and Simulation of a Microsuction Cup Integrated with a Valveless Piezoelectric Pump for Robotics

Bingshan Hu[1,2] **and Hongliu Yu**[1,2]

[1] *University of Shanghai for Science and Technology, Shanghai 200093, China*
[2] *Shanghai Engineering Research Center for Assistive Devices, Shanghai 200093, China*

Correspondence should be addressed to Bingshan Hu; icebergh@126.com

Received 4 January 2018; Revised 14 May 2018; Accepted 6 June 2018; Published 27 June 2018

Academic Editor: Simone Cinquemani

The traditional suction mechanism with an air pump in robotics is difficult to miniaturize. Integrating a piezoelectric pump into a suction cup is an effective method to achieve miniaturization. In this paper, a novel suction cup with a piezoelectric micropump is designed. The micropump is valveless and the suction cup is designed with a laminated structure in order to facilitate miniaturizing and manufacturing. A systematic optimization design method of the suction cup is introduced which addresses the static and dynamic driving characteristics of the piezoelectric actuator and the rectifying efficiency of diffuser/nozzle's optimization. The design is verified via simulation using an improved equivalent electric network model. Static lumped parameters in this model are calculated by the finite element method instead of the traditional analytic method, and the diffuser/nozzle's flow resistance is computed by integrating and introducing rectifying efficiency coefficient. Simulation results indicate that the suction cup can generate a stable negative pressure, and the equivalent electric network model can improve the simulation efficiency and accuracy. The maximum steady-state negative pressure of the suction cup can also be effectively improved after optimization.

1. Introduction

Suction technology is widely used in robotics. By installing a suction cup at the end of a manipulator, numerous forms of work, such as pickup and handling, can be realized. If the suction device is installed on the mobile mechanism of a robot, the robot can move freely on different walls. Magnetic suction requires that the object or the wall to be suctioned must be composed of a magnetic conducting material, which limits the application scope [1]. With technology progression, there have been some new suction mechanisms such as electrostatic and dry adhesive [2], but they have not been used at a large scale. In order to prevent air leakage, negative pressure suction is generally used to suck objects with flat surfaces, such as glass, LCD panels, packaged products, but it cannot be applied to arcs, grooved surfaces, and small objects [3]. To achieve the grasping of different planes and sizes, an effective strategy is to reduce the size of the suction cup to form a suction cup array to fit objects at different sizes and surfaces [4]. In addition, with the development of micro mobile robot application, miniaturized wall climbing robots need to be designed to enter a narrow space to perform tasks. Therefore, it is important to develop micro negative pressure suction mechanism for robot operation or movement.

To produce negative pressure in a suction cup, one method is to increase the volume of the suction cup through a mechanical device when the air quantity and temperature in the suction cup is constant, and this is called a passive suction cup. Because there is not a traditional air pump, the suction cup's size can be miniaturized. Takahiro Matsuno has developed a passive suction cup based on a motor-actuated disc spring [5]. Experiments show that a suction cup with an outer diameter of 120 mm can produce a maximum suction force of 60 N, and the negative pressure can be maintained for 200 s [5]. To reduce the volume of the passive suction cup further, Hu [6] has designed a miniature passive suction cup based on a shape memory alloy (SMA) actuator, and the principle is to heat the shape memory alloy spring to make the elastomer material deform. The geometric size of the suction cup is 28 mm × 26.8 mm, and its weight is 29 g.

Experimental results show that the suction cup has a large power consumption and a slow negative pressure response [6]. Huashan Feng [7] has developed a passive suction actuated by ion-exchange polymer metal composite (IPMC) and the suction cup can reduce the power consumption effectively compared to the SMA actuated suction cup [7]. Because it is difficult to ensure a complete seal, the biggest drawback of the passive negative pressure suction cup is that when there is an air leakage, the negative pressure will disappear quickly.

The other way is to reduce the air quantity in a suction cup under the condition that the volume and temperature of the air in the suction cup are constant. This is the basic principle of using an air pump to extract air from a suction cup to produce negative pressure. T. Takahashi [8] designed a flexible vacuum gripper with miniature-arrayed valves based on MEMS technology. This gripper can hold a free-form surface, such as steps and curvatures, but the gripper still requires use of traditional vacuum pumps [8]. The traditional reciprocating or rotary vacuum pumps are difficult to miniaturize. A kind of thin film micropump is widely used in the field of microfluidic control, which can realize directional transmission of flow state materials. Olsson [9] designed a gas micropump with two piezoelectric actuators, a vibrating cavity and two dynamic valves. Results show that the maximum net flow of the micropump is up to 8 ml/min, and the geometric size of the micropump is $20 \times 16 \times 2.3$ mm [9]. The robust design method of the gas micropump has been studied by Richte [10].

If the above thin film micropump can be integrated into a small suction cup, it can overcome the shortcoming of the passive suction cup. At the same time, the volume of the suction cup can be reduced and a stable negative pressure produced. In this paper, a micro negative pressure suction cup integrated with a piezoelectric valveless micropump is designed and its negative pressure response studied by simulation. The negative pressure generation principle of the suction cup is analyzed, and a micro negative pressure suction cup with an integrated valveless piezoelectric pump is designed in detail. Then, the process to optimize the design of the suction cup is presented. Following the optimization process, an equivalent electric network model of the suction cup is formulated, and the suction characteristics of the suction cup are studied via simulation.

2. Design of the Suction Cup with Micropump

2.1. Structure Design of the Suction Cup. To make the micropump have good air transmission characteristics, the pressure difference dP in the pump cavity must be increased as much as possible [11]. The pressure change of the air in the micropump is

$$dP = \frac{-dV/V}{\kappa}. \quad (1)$$

In (1), κ is the compression rate, dV is the volume change, and V is the initial volume of the air. In order to increase dP in a gas micropump, it is necessary to reduce the initial volume V and increase the volume change dV of the gas in the micropump at the same time. The most direct way to reduce V is to reduce the thickness of the vibrating cavity as much as possible. If the thickness of the vibrating cavity is smaller than the deflection of the piezoelectric actuator, the vibrating cavity wall will prevent further deformation of the piezoelectric actuator. In addition, a very thin vibrating cavity is difficult to manufacture. The volume change dV is decided by the micropump actuator. In the choice of the actuator, the piezoelectric actuator has a comprehensive performance advantage in response time, power consumption, and reliability. Compared with the piezoelectric stack actuator, the unimorph circular piezoelectric actuator has a smaller volume, larger output displacement, and shorter response time, and it is more suitable for driving the suction cup with a micropump [12]. To increase the volume change dV, the unimorph circular piezoelectric actuator is chosen for the suction cup with micropump.

To increase the gas volumetric change rate dV/V further, two piezoelectric actuators can be installed on two sides of one vibrating cavity, which is different with the traditional micropump [9]. When two actuators deform at the same time, the volumetric change rate is increased [9].

The micropump in this paper uses a diffuser and a nozzle instead of valves, and the reason is that the valve needs a pressure difference to open, so the pressure in the vibrating cavity will be partially lost. Reliability is reduced due to wear and fatigue of mechanical parts of the valve. The structure of the micropump with valve is also more complex and not easy to manufacture and assemble and is not conducive to reducing the volume size and weight of the micropump suction cup. A valveless micropump overcomes the above shortcoming and has a greater development prospect. Currently most valveless micropumps use cone-shaped tubes to guide the fluid. Compared with the spatial cone-shaped tube, and the manufacturing process of the plane cone tube is simpler and is beneficial to integrate with other microdevices [13]. Therefore, a planar cone tube will be used in the micropump suction cup in this paper.

Representative geometric dimensions of the gas micropump from the literature [9] are in Table 1. It can be seen that some key dimensions are very small. This makes them difficult to manufacture by traditional methods, but the air transmission characteristics of the micropump are very sensitive to these dimensions. If the micropump is assumed to be laminated by several thin layers, which can be manufactured independently, the micropump processing difficulty will be greatly reduced [14]. Therefore, the suction cup with micropump in this paper is designed with a laminated structure; the smaller parts are machined by laser engraving, while the other parts are processed by traditional machining methods.

The suction cup designed in this paper is shown in Figure 1. It is divided into upper and lower covers, upper and lower elastic substrates, upper and lower piezoelectric material layer, vibrating cavity layer, and suction chamber layer. The upper and lower covers are made by the traditional mechanical processing method, and they are made of polymethyl methacrylate. There are grooves on the upper and lower covers. The central circular groove is used to

Table 1: Geometric sizes of a gas micropump [9].

	Item	Data
Piezoelectric actuator	Piezoelectric material layer radius R_1 (mm)	5
	Piezoelectric material layer thickness h_p (mm)	0.2
	Elastic substrates radius R_2 (mm)	6
	Elastic substrates thickness h_m (mm)	0.15
Cone tube	Expanding length L (mm)	3
	Minimum section width d_a (mm)	0.12
	Maximum section width d_b (mm)	0.64
	Expanding angle θ (°)	10
	Depth h_a (mm)	0.1
Vibrating cavity	Radius (mm)	6
	Depth (mm)	0.1

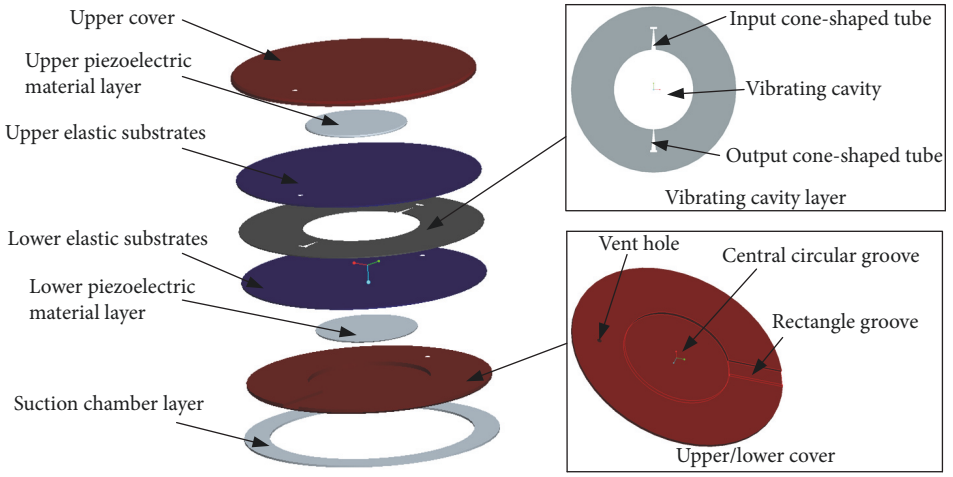

(a) Exploded view

(b) Sectional view

Figure 1: Structure diagram of the suction cup with micropump.

reserve space for deforming of the piezoelectric actuator, and the other rectangle groove is used for the wiring of the piezoelectric actuator. The upper and lower elastic substrate is made of copper plate, which is easy to deform. One side of the substrate is adhered to a piezoelectric material layer and the other side to the vibrating cavity layer. A vibrating cavity, an input cone-shaped tube, and an output cone-shaped tube are engraved by laser on the vibrating cavity layer. The material of the vibrating cavity layer is stainless steel. The suction chamber layer is manufactured with a soft silicone rubber plate, whose sealing performance is satisfactory, and it is attached to the lower cover.

There are vent holes on the upper/lower covers and the upper/lower elastic substrates, respectively. The maximum section end of the input cone tube is connected to the vibrating cavity, and then the minimum section end of the input conical tube, lower substrate vent hole, lower cover vent hole, and the suction cavity are connected in series. The upper cover vent hole, the upper elastic substrates vent hole, and the maximum section end of the output conical tube are connected in series. The minimum section end of the output conical tube is connected to the vibrating cavity. The upper cover vent hole is connected to the outside atmosphere.

2.2. Description of Working Principle. The working principle of the micropump suction cup is shown in Figure 2. Under the excitation of the AC electric field signal, piezoelectric actuators make the volume of the vibrating cavity larger or smaller periodically. When the volume of the vibrating cavity increases, the air in the suction cavity and the external

environment flows into the vibrating cavity simultaneously through the input cone tube and the output cone tube. This is called the inhalation process. In this process, the effect of the input cone tube is equivalent to a diffuser, while the output cone tube is equivalent to a nozzle. Through a proper design of geometric parameters of cone tubes, the flow resistance through the diffuser is less than through the nozzle. Therefore, the air from the suction cavity into the vibrating cavity is more than the air from the outside, and the micropump is in "supply mode." When the volume of the vibrating cavity is reduced, the air flows out of the vibrating cavity, and the air entering the suction cavity from the vibrating cavity is less than that from the vibrating cavity to the outside air. The micropump is then in "pumping mode." When the volume of the vibrating cavity changes continuously due to the vibration of piezoelectric actuators, a continuous differential flow is generated, and the air in the suction cavity is continuously extracted, resulting in the formation of negative pressure in the suction cavity.

3. Optimization of the Suction Cup with Micropump

In the second section, a valveless micropump suction cup which is easy to be processed and has large volumetric change rate is designed. In order to further improve the performance of the micropump suction cup, a systematic optimization design method is introduced in this section, which covers the optimization of static and dynamic driving characteristics of piezoelectric actuators and rectifying efficiency of diffuser/nozzle.

3.1. Piezoelectric Actuator Optimization. Research shows that the geometric size, material properties, driving voltage, and driving frequency affect the deformation of a piezoelectric actuator. The geometric size and material properties affect static driving characteristics, that is, the relationship between the driving electric field and the deformation, while the driving frequency will affect the dynamic driving characteristics [15].

3.1.1. Static Driving Characteristics Optimization. The structure of the unimorph circular piezoelectric actuator used in the micropump suction cup is shown in Figure 3, and it can be divided into two parts, which consist of a piezoelectric layer with a radius of R_1 and a copper substrate layer with a radius of R_2. Their thicknesses are h_p and h_m, respectively.

Research shows that there is an optimal radius ratio R_1/R_2 and an optimal thickness ratio h_m/h_p, which makes the deformation of the piezoelectric actuator maximum at the same driving voltage [15]. In this paper, the geometric size of the actuator is optimized based on the theoretical mechanics model of the piezoelectric actuator.

When a DC voltage U is applied to the piezoelectric actuator, the approximate analytical solution of the piezoelectric actuator's deflection is [16]

$$\varpi(r) = \begin{cases} \varpi_1(r) = \dfrac{C_1\left\{2R_1^2\ln\left(R_1/R_2\right) + \left[1-\left(R_1/R_2\right)^2\right]r^2\right\}U}{C_2 - C_3\left(R_1/R_2\right)^2 + (1/2)\,h_p^4 S_m^2\left(1+\upsilon_p\right)\left(R_1/R_2\right)^4}, & r \le R_1 \\ \varpi_2(r) = \dfrac{C_1\left\{2R_1^2\ln(r) - R_1^2\left[2\ln\left(R_2\right)-1\right] - \left(R_1/R_2\right)^2 r^2\right\}U}{C_2 - C_3\left(R_1/R_2\right)^2 + (1/2)\,h_p^4 S_m^2\left(1+\upsilon_p\right)\left(R_1/R_2\right)^4}, & R_1 \le r \le R_2. \end{cases} \tag{2}$$

In (2), υ_p is Poisson's ratio of the piezoelectric material, and S_m is elastic compliance constant of the copper substrate.

The constants C_1, C_2, and C_3 are

$$C_1 = 3d_{31}h_m S_{11}^E S_m\left(h_m + h_p\right) \tag{3}$$

$$C_2 = 4S_{11}^E h_p h_m^3 S_m + 6S_{11}^E h_m^2 h_p^2 S_m + 4S_{11}^E h_m h_p^3 S_m + \frac{1}{2}h_p^4 S_m^2\left(1+\upsilon_p\right) + \frac{2h_m^4 S_{11}^{E2}}{1+\upsilon_p} \tag{4}$$

$$C_3 = 4S_{11}^E h_p h_m^3 S_m + 6S_{11}^E h_m^2 h_p^2 S_m + 4S_{11}^E h_m h_p^3 S_m + h_p^4 S_m^2\left(1+\upsilon_p\right). \tag{5}$$

In (3)–(5), d_{31} and S_{11}^E are the piezoelectric constant and elastic compliance constant for the piezoelectric layer.

By (2)–(5), the volume change of the vibrating cavity caused by one unimorph circular piezoelectric actuator can be obtained when a DC voltage U is applied:

$$\Delta V = \int_0^{R_1} \varpi_1(r)\,2\pi r\,dr + \int_{R_1}^{R_2} \varpi_2(r)\,2\pi r\,dr. \tag{6}$$

According to the analytical solution in (6), the optimal radius ratio and thickness ratio are found based on the geometry size of the piezoelectric actuator as shown in Table 1. Figure 4 shows the relationship between volume changes and geometric dimensions of the piezoelectric actuator; Figure 4(a) is the volume change curve of the vibrating cavity after a 30 V DC voltage is applied. The thickness of the piezoelectric material and the copper substrate is 0.2 mm and 0.1 5mm, respectively. The radius of the copper substrate varies between 0 and 0.02 m, and the radius ratio R_1/R_2 varies between 0 and 1. From Figure 4(a), it can be seen that when the radius ratio is constant, the volume change will increase with the increase of the radius of the copper substrate. The reason is that when the radius is larger, the piezoelectric

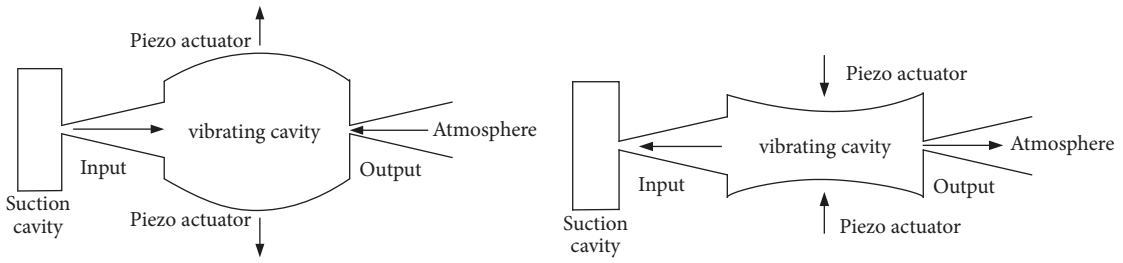

(a) Supply mode (b) Pump mode

Figure 2: Working principle of the micropump suction cup.

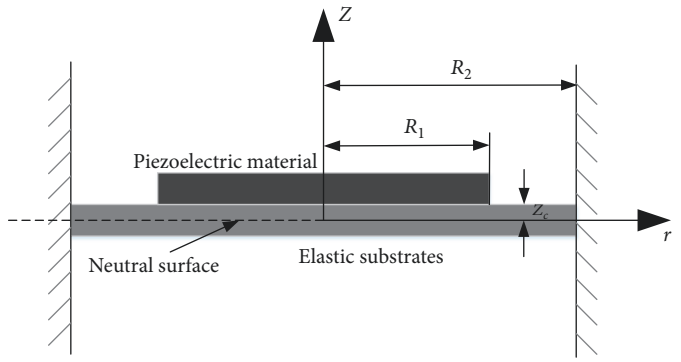

Figure 3: Schematic diagram of a unimorph circular piezoelectric actuator.

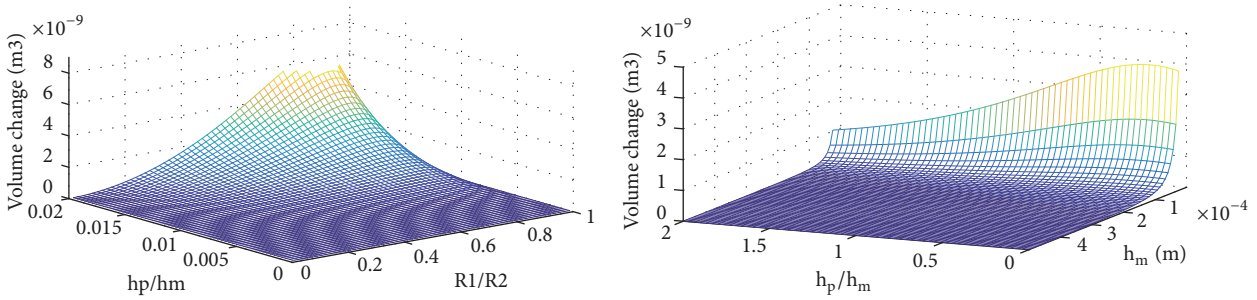

(a) Optimization of radius ratio (b) Optimization of thickness ratio

Figure 4: Static driving characteristics optimization of piezoelectric actuator.

composite plate will deform more easily. When the radius of the copper substrate is constant, there is an optimal radius ratio, which makes the volume change the maximum under the same driving voltage. The radius ratio is approximately 0.94. When the radius of the copper substrate is small, the radius ratio has little influence on the volume change, and the radius of the copper substrate should be greater than 10 mm.

In Figure 4(b), the radius of the piezoelectric material and the copper substrate is 5 mm and 6 mm, respectively. The thickness of the copper substrate changes between 0 and 0.5 mm, and the thickness ratio of the piezoelectric material and the copper substrate varies from 0 to 2. From Figure 4(b), it can be seen that when the thickness of copper substrate is large, the volume change is not obvious, and the thickness ratio has little influence on volume change. This is because the larger the thickness of copper substrate is, the more difficult the deformation of piezoelectric composite plate is, and the thickness of copper substrate should be less than 0.2 mm. When the thickness of the copper substrate is small, there is an optimal thickness ratio, which makes the volume change be the largest under the same driving voltage, and the thickness ratio is 0.17.

3.1.2. Dynamic Driving Characteristics Optimization. In order to produce a stable negative pressure, an alternating voltage should be applied on piezoelectric actuators to make it vibrate continuously. In the past, most work on dynamic driving characteristics of piezoelectric actuators used the finite element method to solve for the resonant frequency, and few studies have been done on the dynamic changes of the piezoelectric actuator's volume change under an alternating electric field. In this section, an equivalent circuit model

of piezoelectric actuator based on lumped parameter is formulated to simulate the dynamic driving performance of the piezoelectric actuator and thereby select the best driving frequency. Additionally, it also lays a foundation for the simulation of the negative pressure response of the suction cup with micropump.

If the alternating power is V_{ac}, the equivalent displacement along the polarization direction of the actuator is x, and the equivalent output force is F. The electrical charge at both ends of the piezoelectric layer is q, and the surface area of the piezoelectric actuator is A. According to the first kind of piezoelectric equation, the following equation can be obtained [17]:

$$\begin{bmatrix} \frac{x}{h_p} \\ \frac{q}{A} \end{bmatrix} = \begin{bmatrix} S^{EE} & d^E \\ d^E & \xi^{TE} \end{bmatrix} \begin{bmatrix} \frac{F}{A} \\ \frac{V_{ac}}{h_p} \end{bmatrix}. \tag{7}$$

In (7), S^{EE}, d^E, and ξ^{TE} are, respectively, equivalent compliance constant, equivalent piezoelectric constant, and equivalent dielectric constant of the piezoelectric actuator along the direction of deflection. Under small deformations, it can be approximately considered that $\Delta V = xA$, and (7) can be transformed into

$$\begin{aligned} \begin{bmatrix} \Delta V \\ q \end{bmatrix} &= \begin{bmatrix} S^{EE} h_p A & d^E A \\ d^E A & \frac{A\xi^{TE}}{h_p} \end{bmatrix} \begin{bmatrix} P \\ V_{ac} \end{bmatrix} \\ &= \begin{bmatrix} C_{AS} & d_A \\ d_A & C_{EF} \end{bmatrix} \begin{bmatrix} P \\ V_{ac} \end{bmatrix}. \end{aligned} \tag{8}$$

In (8), C_{AS} is the volume change caused by a unit pressure on a piezoelectric actuator when the driving voltage is zero.

$$C_{AS} = S^{EE} h_p A = \left. \frac{\Delta V}{P} \right|_{V_{ac}=0} = \frac{\int_0^{R_2} \varpi(r)|_{V_{ac}=0} \, 2\pi r \, dr}{P}. \tag{9}$$

The constant d_A describes the volume change caused by a unit drive voltage when the applied pressure is zero.

$$d_A = d^E A = \left. \frac{\Delta V}{V_{ac}} \right|_{P=0} = \frac{\int_0^{R_2} \varpi(r)|_{P=0} \, 2\pi r \, dr}{V_{ac}} \tag{10}$$

According to the definition of (9) and (10), the constants C_{AS} and d_A can be calculated. Due to the dielectric properties of the piezoelectric material, there is a free capacitance for the unimorph circular piezoelectric actuator, and it can be calculated as

$$C_{EF} = \frac{\pi R_1^2 \xi^{TE}}{h_p} \tag{11}$$

Because of the direction of the electric field, the deflection direction and the polarization direction of the piezoelectric material are the same, and the equivalent dielectric constant ξ^{TE} is approximately equal to ξ_{33}.

In order to obtain the two ports' equivalent circuit model of the piezoelectric actuator, (8) is differentiated with respect to time and Laplace transformation is carried out, which yields

$$\begin{bmatrix} Q \\ i \end{bmatrix} = \begin{bmatrix} j\omega C_{AS} & j\omega d_A \\ j\omega d_A & j\omega C_{EF} \end{bmatrix} \begin{bmatrix} P \\ V_{ac} \end{bmatrix} \tag{12}$$

In (12), Q is the volume change of the piezoelectric actuator in a unit time (volume change velocity); i is the equivalent current flowing through the piezoelectric material layer; and ω is frequency. Equation (12) can be represented as a two ports' equivalent circuit as shown in Figure 5(a) [17]. Due to the electromechanical coupling effect of piezoelectric actuators, an ideal transformer is used to describe the coupling effect in Figure 5. The right side of the transformer is lumped elements in fluid domain, and the other side is the electrical domain lumped elements. The parameter ϕ is the fluid electrical coupling coefficient.

Assuming that the current of the right side of the transformer in Figure 5(a) is i_0, then, at the electrical domain side,

$$i = j\omega C_E V_{ac} + i_0 = j\omega C_E V_{ac} - \phi Q \tag{13}$$

At the fluid domain side

$$P = \frac{Q}{j\omega C_M} + \phi V_{ac} \tag{14}$$

According to (14),

$$Q = j\omega C_M P - j\omega C_M \phi V_{ac} \tag{15}$$

By comparing (15) and (12), we can get the parameters C_M and ϕ:

$$\begin{aligned} C_M &= C_{AS}, \\ \phi &= -\frac{d_A}{C_{AS}} \end{aligned} \tag{16}$$

Substituting (15) and (16) into (12),

$$i = j\omega d_A P + j\omega \left(C_E + \frac{d_A^2}{C_{AS}} \right) V_{ac} \tag{17}$$

By comparing (17) and (12), the blocked electrical capacitance C_E can be gotten:

$$C_E = C_{EF} - \frac{d_A^2}{C_{AS}} \tag{18}$$

When the driving frequency is very low, it is not essential to consider the influence of the piezoelectric actuator's quality on driving characteristics, but when the driving frequency increases, the quality affects the vibration of the piezoelectric actuator [18]. On the basis of Figure 5(a), an equivalent inductance M_M representing mass inertia is added to the fluid domain side, and the formula for calculating M_M is [17]

$$M_M = 2\pi \int_0^{R_2} \rho_A \left(\left. \frac{\varpi(r)}{\Delta V} \right|_{V_{ac}=0} \right)^2 r \, dr \tag{19}$$

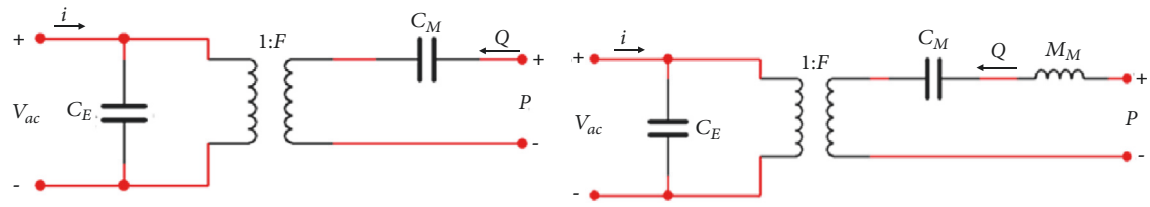

(a) Not considering the influence of the inertia

(b) Considering the influence of the inertia

Figure 5: Two-port equivalent circuit of the piezoelectric actuator.

In (19), ρ_A is the areal density of the piezoelectric composite plate. The equivalent circuit considering the influence of inertia is shown in Figure 5(b).

In order to establish the equivalent circuit model of the piezoelectric actuator in micropump suction cup in detail, lumped parameters should be calculated first. In many studies, the analytic method is used directly in the calculation of the lumped parameters [17]. The accuracy of the parameters depends entirely on the accuracy of the theoretical model. However, the exact theoretical model is often difficult to establish, and even if it is established, its numerical calculation process is complex. In this work, the finite element method is used instead to calculate some static parameters according to their physical meaning to improve the accuracy of the equivalent circuit model, such as C_{AS}, d_A, and M_M.

Geometric parameters of the piezoelectric actuator before optimization are in Table 1. First, C_{EF} can be calculated directly, and $C_{EF} = 3.7515e-009\ \mathrm{C^2J^{-1}}$. According to the definition of d_A, the finite element model of piezoelectric actuator is established using ANSYS 10.0. In the model, a unit driving voltage is applied, and the external pressure load on the actuator is zero. The volume change ΔV is calculated by ANSYS 10.0, then d_A can be obtained by (10), and $d_A = -1.5275e-012\ \mathrm{m^3CJ^{-1}}$. Then the load applied on the finite element model is changed. A unit external pressure load is applied on the finite element model, and the driving voltage is zero. C_{AS} can be calculated by its definition, and $C_{AS} = 4.6201e-015\ \mathrm{m^6J^{-1}}$; the equivalent inductor M_M can be obtained by the same method, and $M_M = 3.2061e4\ \mathrm{Js^2m^{-6}}$. Finally, C_M, ϕ, and C_E can be obtained according to (16) and (18), and $C_M = 4.6201e-015\ \mathrm{m^6J^{-1}}$, $\phi = 337.935\ \mathrm{Cm^{-3}}$, and $C_E = 3.2353e-009\ \mathrm{C^2J^{-1}}$. The equivalent circuit model can be obtained by replacing the above lumped parameter into Figure 5(b). It is modeled in circuit simulation software Multisim 10.0 as shown in Figure 6. A capacitance C1 is added to the fluid domain side to integrate volume change velocity Q, and the volume change of the piezoelectric actuator ΔV is obtained.

In order to verify the correctness of the two ports' equivalent electric network model, the finite element method is used to simulate the transient driving characteristics of the piezoelectric actuator, and the software ANSYS 10.0 is used. The voltage load is applied to the piezoelectric material layer. Then the FULL method in ANSYS is applied to analyze the transient dynamics of the piezoelectric actuator. Because the finite element method for transient dynamic analysis is very time-consuming, the dynamic response just in the first 0.2 ms is analyzed. The displacement along the polarization direction of the piezoelectric material is kept in analysis results, and then the volume change is calculated. Figure 7 is the comparison of results of the finite element analysis and the equivalent electrical network analysis in this period. It can be seen from the diagram that simulation results by two methods are basically the same, so the correctness of the two ports' equivalent electric network model is verified.

Using the equivalent electric network model and the simulation software Multisim 10.0, the steady-state volume change amplitude of the piezoelectric actuator can be obtained at different driving frequencies as shown in Figure 8. Curve 1 in Figure 8 is the steady-state volume change amplitude's frequency response curve of the original piezoelectric actuator. The amplitude of the driving voltage is 30 V. As can be seen from Figure 8, the resonant frequency is 13060 Hz which makes the actuator's steady-state volume change amplitude the largest, and the frequency is very close to the first-order resonant frequency of the piezoelectric actuator obtained by finite element method. This further validates the correctness of the equivalent electric network model.

In Figure 8, curve 2 is the frequency response curve of the steady-state volume change amplitude after the radius ratio is optimized. Curve 3 is the frequency response curve of the steady volume change amplitude after thickness optimization. In curves 2 and 3, the amplitude of the driving voltage is 30V. After the geometric parameters are changed, the parameters in the equivalent circuit model are recalculated and simulations are carried out. Compared with these curves, it is known that, after optimizing the radius ratio and thickness ratio, the maximum value of the steady-state volume change amplitude of the piezoelectric actuator at the first resonance frequency is increased, and the first-order resonance frequency has also changed. When the thickness ratio is optimized, the first-order resonance frequency decreases to 4 kHz, but the maximum amplitude of the steady-state volume change increases to 1.3 μL. When the radius ratio is optimized, the first-order resonance frequency rises to 13350 Hz, and the maximum amplitude of the steady-state volume change increases to 1.8 μL.

The radius and thickness ratio of curve 4 are not optimized, but the amplitude of the driving voltage is 50 V. The comparison between curve 1 and curve 4 shows that the

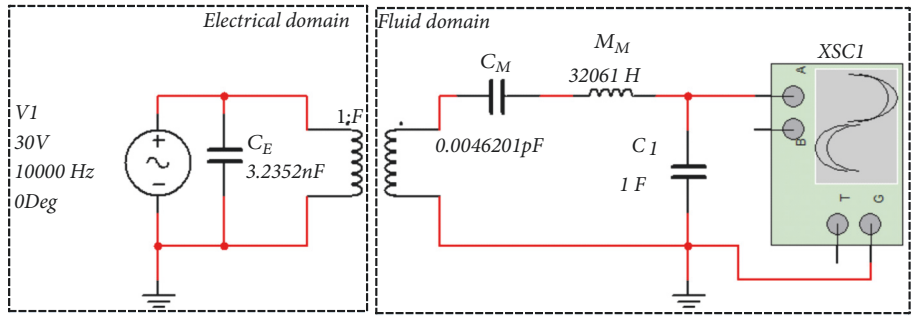

Figure 6: Piezoelectric actuator's equivalent circuit model.

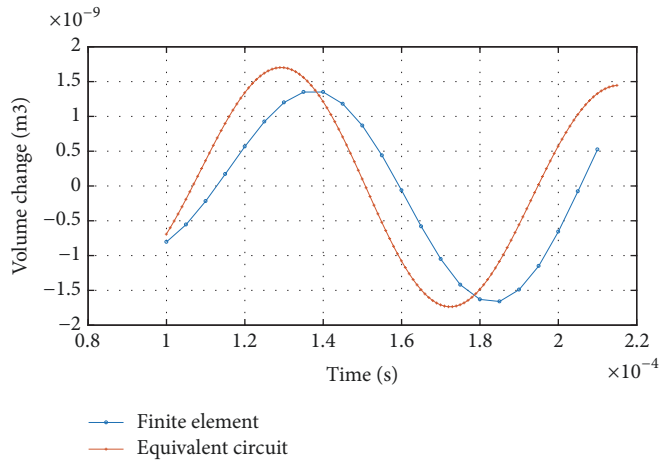

Figure 7: Correctness verification of the two ports' equivalent electric network model.

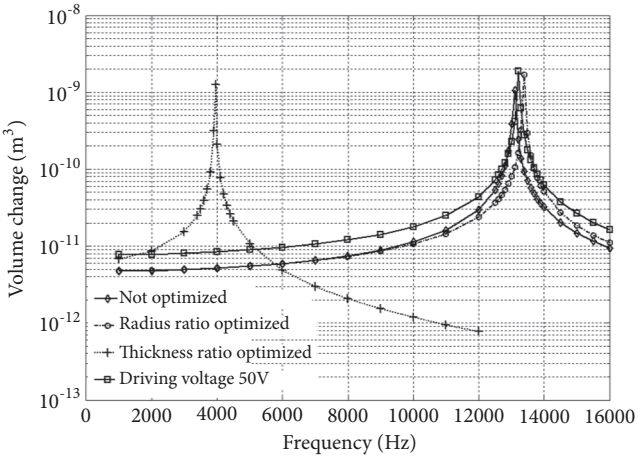

Figure 8: Frequency response curve of the steady-state volume change amplitude.

larger the driving voltage, the larger the volume change. The maximum value of the steady-state volume change at the driving voltage 50 V is approximately 1.9 μL.

3.2. Diffuser/Nozzle Optimization. The air rectifying characteristics of the cone-shaped tube have an extremely important influence on the performance of the micropump suction cup, so the cone tube must be optimized. The rectification efficiency is defined as

$$\varepsilon(p) = \frac{Q_d(p) - Q_n(p)}{Q_d(p) + Q_n(p)} \tag{20}$$

Q_d and Q_n are air volume flows through the cone-shaped tube along the direction of expansion and contraction, respectively.

As shown in Figure 9, θ, L, d_a, d_b, and h are the plane cone tube's expanding angle, expanding length, minimum section width, and maximum section width and depth. It is very difficult to study the cone tube's transport characteristics of air from a theoretical or experimental point of view accurately, so a Computational Fluid Dynamics module in ANSYS 10.0 is used to analyze the influence of expanding angle, expanding length, and section width on the rectification efficiency to optimize the design of the conical tube. Separation and reflux are easy to occur when the air flows along the direction of expansion, as the cross-section increases, and the flow along the contraction direction is more stable. Therefore, the flow state of air in the diffuser can be set as a turbulent or turbulent mixed flow, which needs to open the turbulence analysis module in finite element analysis software. The air flow in the nozzle can be set as a laminar flow [19]. Further, the air flow is considered to be incompressible and axisymmetric in the process of analysis. Considering the constraints of computer

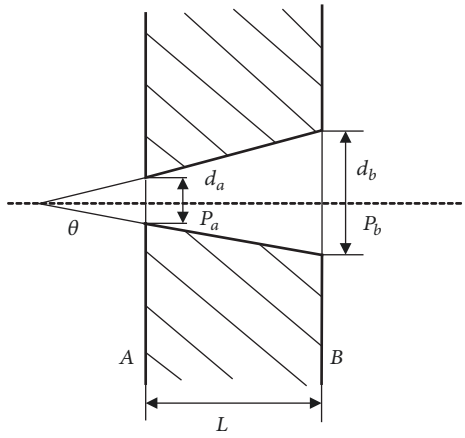

Figure 9: Structure chart of the plane cone tube.

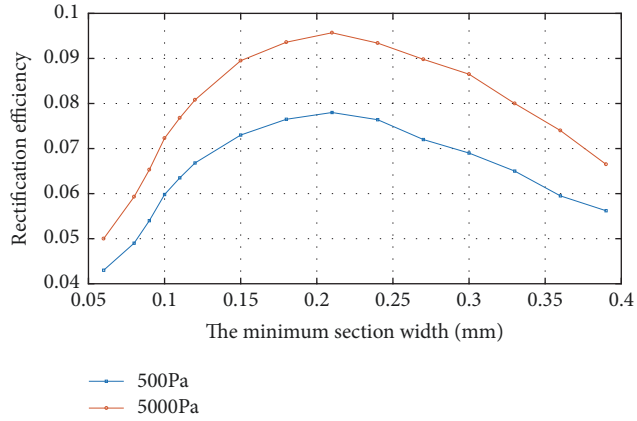

Figure 10: Relationship between the minimum section width and the rectification efficiency.

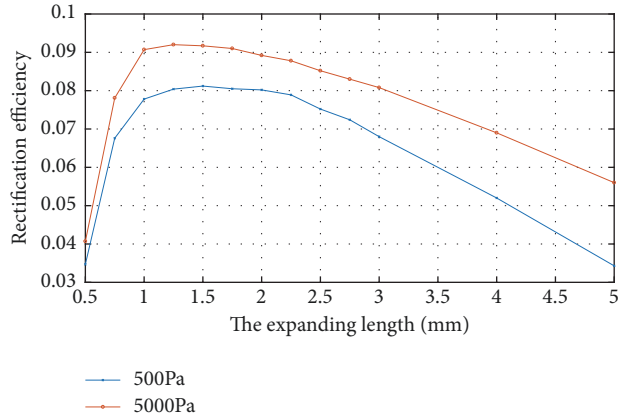

Figure 11: Relationship between the expanding length and the rectification efficiency.

hardware and computing time, a two-dimensional finite element model is used to analyze the flow field characteristics in a cone tube.

On the basis of Table 1, the size of expanding length, minimum section width, and expanding angle are changed, respectively. Then, the corresponding finite element model is set up to investigate the influence of the geometric size change on the air rectification efficiency of the cone tube.

In order to calculate the rectification efficiency, the volume flow must be known, and it can be calculated by the following equation in the finite element model:

$$Q = \int_0^{d_a} v_{ave} h dx = \sum_{i=0}^{n} v_i h \Delta x \tag{21}$$

In (21), v_{ave}, v_i, Δx, and n are average velocity, velocity of each finite element, width of each finite element, and number of finite elements at the minimum section of the cone tube's finite element model, respectively. v_i can be read out during the postprocessing of finite element analysis. Through (21), Q_d and Q_n are calculated, and the rectification efficiency of a cone-shaped tube can be obtained.

3.2.1. Influence of the Minimum Section Width. To investigate the effect of the minimum section width on the rectification efficiency, the expanding length and expanding angle are fixed at 3 mm and 10 degrees. The minimum section width varies from 0.06 mm to 0.36 mm. The pressure difference between the two ends of the cone tube is 0.5 kPa and 5.0 kPa. Initially, the rectification efficiency is simulated by ANSYS 10.0 in different situations, and then all simulation results are shown in Figure 10 with the data processing software Origin Pro 9.0. The graph shows that there is an optimal minimum section width, which makes the rectification efficiency the highest and the optimal minimum section size is not affected by the pressure difference. The optimal minimum section width is 0.21 mm, and the rectifying efficiency is 0.095 when the pressure difference is 5 kPa.

3.2.2. Influence of the Expanding Length. To investigate the effect of expanding length on the rectification efficiency, the minimum section width and expanding angle are fixed at 0.12 mm and 10 degrees. The expanding length varies from 0.5 mm to 5.0 mm. The pressure difference between the two ends of the cone tube is 0.5 kPa and 5.0 kPa, and simulation results are shown in Figure 11. It can be seen from the figure that when the pressure difference is fixed, the rectification efficiency increases with the increase of the expanding length. When the expanding length is about 1.5 mm, the rectification efficiency reaches the maximum. When expanding length increases from 1.5 mm to 2.5 mm, the rectification efficiency decreases slightly. If the expanding length continues to increase, the rectification efficiency decreases. The reason is that the conversion efficiency between the kinetic energy and potential energy of the cone tube is very low when the expanding length is short. With the increase of expanding length, the conversion efficiency increases. From 1.5 mm to 2.5 mm, the speed of energy conversion is relatively stable, so the rectification efficiency is relatively stable. If the expanding length continues to increase, the main section will continue to expand along the direction of expanding. In this way, the airflow is easy to move along the reverse direction of the diffuser and form a vortex area. As shown in

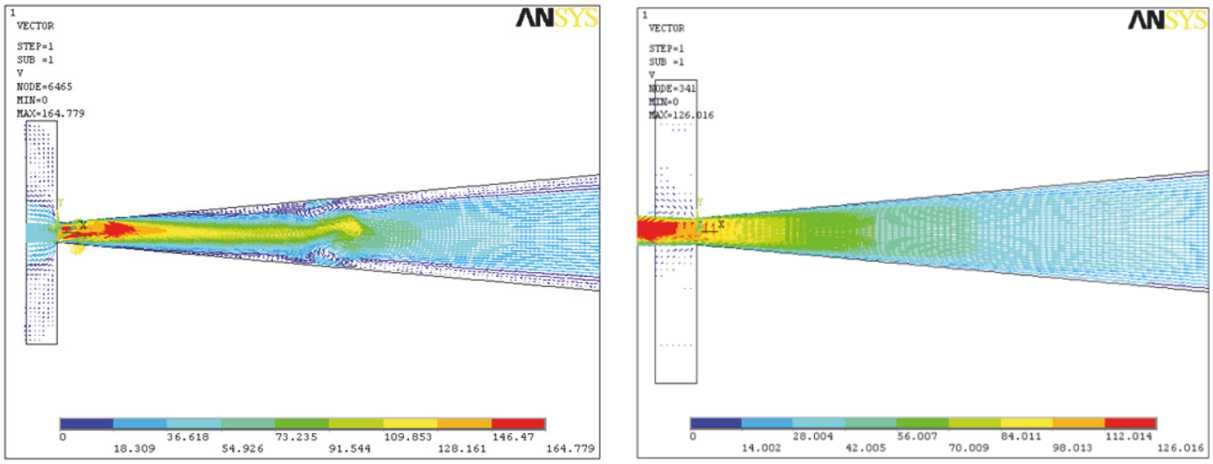

(a) Diffuser (b) Nozzle

Figure 12: Flow field vector diagram in the conical tube.

Figure 12(a) which is obtained by ANSYS, the vortex appears in diffuser when the expanding length is 5 mm and the pressure difference is 5 kPa. In the direction of contraction, the above situation will not appear, because the cone tube's section becomes smaller (Figure 12(b)). These reasons lead to a decrease in the rectification efficiency of the cone tube.

3.2.3. Influence of the Expanding Angle. To investigate the effect of expanding angle on the rectification efficiency, the minimum section width and expanding length are fixed at 0.12 mm and 3 mm. The expanding angle varies from 6° to 16°. The pressure difference between the two ends of the cone tube is 0.5 kPa and 5.0 kPa, and simulation results are shown in Figure 13. The figure shows that there is an optimal expanding angle to maximize rectification efficiency, and the optimal expanding angle decreases with the increased pressure difference. When the expanding angle is small, the cross-section change of the diffuser is relatively stable, and the transformation from dynamic pressure to static pressure is relatively smooth. When the expanding angle increases gradually, the pressure loss coefficient decreases gradually, so when the expanding angle is less than the optimal expanding angle, the rectification efficiency increases. When the expanding angle increases to larger than the optimal expansion angle, the airflow's dynamic pressure to the static pressure conversion is strong. However, due to the low dynamic pressure of air near the diffuser wall, it is not enough to overcome the rise of static pressure, which leads to the emergence of a vortex similar to Figure 12(a). For the nozzle, the situation described above is not present due to the contraction of the tube wall, so when the expanding angle is larger than the optimal angle, the rectification efficiency decreases gradually. When the pressure difference between the two ends of the diffuser increases, the air velocity in the tube is also greater, and the expanding angle, which can generate a vortex, is smaller, so the optimal expanding angle decreases with the increased pressure difference.

After a large number of finite element analyses, it is found that the minimum section width, expanding angle, and expanding length all have the optimal value to make the air rectification efficiency of a plane cone tube the largest when the other parameters are fixed. At the optimal value, the rectification efficiency increases with the increased pressure difference. This is because when the pressure difference is larger, the flow velocity is higher and the kinetic energy and the pressure potential energy are converted more completely, so at the optimal value the rectification efficiency is higher. The volume change rate of the vibrating cavity and the volume change of the piezoelectric actuator should be maximized to obtain a larger pressure difference.

4. Simulation Study on Negative Pressure Response

In order to verify the rationality of the design of the micropump suction cup, a model should be established to simulate the negative pressure response. Bourouina has discussed a method of establishing the piezoelectric micropump's simulation model by equivalent circuit [19]. The equivalent circuit method can simplify the simulation and analysis process, and the simulation time is short and the efficiency is high compared with the traditional finite element analysis method, but some lump parameters' theoretical calculation processes are complex to get a more exact result. In this paper, to improve the equivalent circuit modeling method, in addition to using the finite element method to calculate static lump parameters as in Section 3.2.1, the computing process of the diffuser/nozzle's flow resistance and inductance is also improved by integrating and introducing rectifying efficiency coefficient, which will be introduced in this section.

4.1. Simulation Model Establishment. Basic components of the micropump suction cup include two unimorph circular piezoelectric actuators, a vibrating cavity, two cone tubes, a suction cavity, and some vents. The equivalent electric network of the piezoelectric actuator has been deduced in Section 3.1.2. Next, the equivalent electrical network model of the vibrating cavity, the suction cavity, and the cone tube

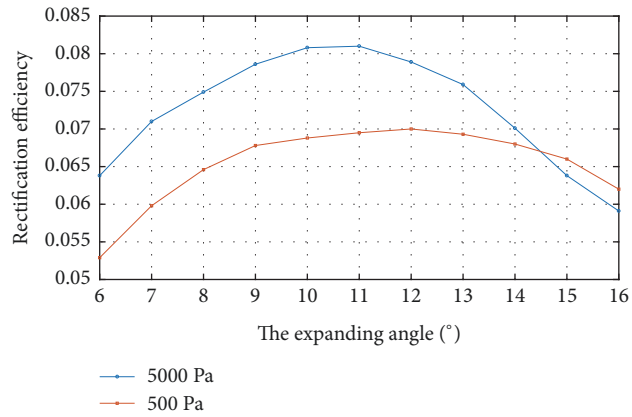

Figure 13: Relationship between the expanding length and the expanding angle.

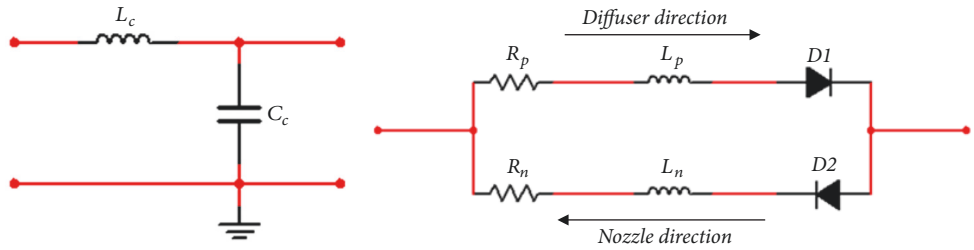

(a) Vibrating cavity and suction cavity (b) Cone tube

Figure 14: Equivalent electric network model of elements.

will be derived. Because the vent hole's length is very short, it is not considered in the equivalent electric network model.

4.1.1. Vibrating Cavity and Suction Cavity. Because the geometric sizes of the vibrating cavity and the suction cavity are relatively large, the flow resistance is ignored. When the air pressure in the cavities changes, the air quantity is different, and this means that the vibrating cavity and the suction cavity have flow capacity. Further, the working frequency of the micropump suction cup is high, and the air pressure changes when the air flows at a high speed in the vibrating cavity and suction cavity, which indicates that these two cavities also have flow inductance.

When the mass of the air in the cavity is m and the section area of the cavity is A_c, the flow resistance is $L_c = m/{A_c}^2$, and the flow capacity is $C_c = \kappa V_0$ [20]. κ and V_0 are the air compressibility and initial volume of the air respectively. The equivalent electrical network model of the vibrating cavity and the suction cavity is shown in Figure 14(a).

4.1.2. Diffuser and Nozzle. The cone tube plays a guiding and rectifying effect on the airflow in the micropump suction cup, and the flow resistance of the air along the nozzle is greater than that of the diffuser. The rectifier element in the electrical circuit is diode. Therefore, in this paper, an ideal diode is introduced to the equivalent circuit of the cone tube to characterize the rectifying effect. Because the length of the cone tube is very short, its air capacity is limited, so the flow capacity is negligible. The flow resistance of a rectangular cross-section microchannel is [21]

$$R_{rect} = \frac{4\mu l}{ab^3}\left(\frac{16}{3} - 3.36\frac{b}{a}\left(1 - \frac{b^4}{12a^4}\right)\right)^{-1} \quad (22)$$

In (22), the length of the rectangle section is $2a$ and $2b$, respectively; μ is the viscosity of the air; l is the length of the microchannel.

Because the cross-sectional area of the plane cone tube is varied, its flow resistance calculation method is different from the traditional fixed section microchannel. As shown in Figure 15, the cross-section width $2a$ at coordinates x along the expanding direction is

$$2a = d_a + \frac{d_b - d_a}{L}x \quad (23)$$

If the depth of the cone tube is 2c, assuming that the width of an infinitely short cone tube is constant, the flow resistance of this infinitely short cone tube can be obtained,

$$R_{d0} = \frac{4\mu}{ac^3}\left\{\frac{16}{3} - 3.36\frac{c}{a}\left(L - \frac{c^4}{12a^4}\right)\right\}^{-1} dx \quad (24)$$

The diffuser's flow resistance R_d can be obtained by integrating (24) along the expanding direction of the diffuser:

$$R_d = \int_0^l \frac{4\mu}{ac^3}\left\{\frac{16}{3} - 3.36\frac{c}{a}\left(L - \frac{c^4}{12a^4}\right)\right\}^{-1} dx \quad (25)$$

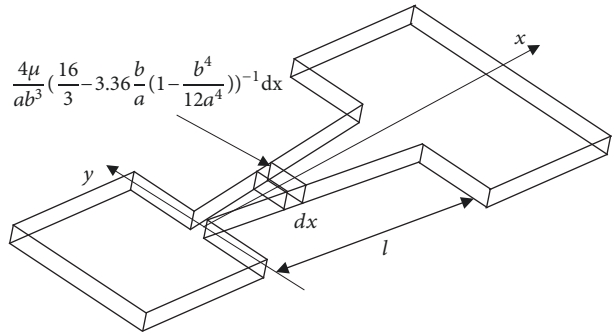

Figure 15: Calculation of cone tube's flow resistance.

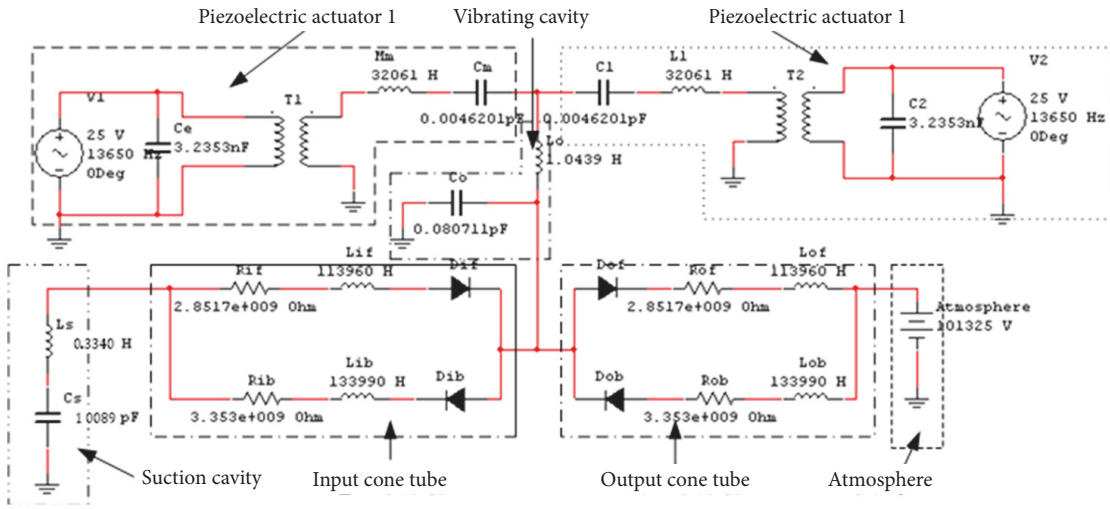

Figure 16: Equivalent electrical network model of the micropump suction cup.

According to the definition of the cone tuber's rectification efficiency, the flow resistance R_n of the nozzle is [18]

$$R_n = \frac{1-\varepsilon}{1+\varepsilon}R_d \tag{26}$$

In (26), the rectification efficiency has been obtained by finite element simulation method. The flow inductance of the microchannel with the same section is [18]

$$L_{hyd} = \frac{\rho l}{A_m} \tag{27}$$

In (27), ρ is the air's line density and A_m is the section area of the microchannel. Using the same calculation method of flow resistance, the flow inductance of diffuser L_d can be obtained:

$$L_d = \rho \int_0^l \frac{dx}{4ac} \tag{28}$$

The flow inductance of nozzle is

$$L_n = \frac{1-\varepsilon}{1+\varepsilon}L_d \tag{29}$$

The final equivalent electrical network model of the cone tube is shown in Figure 14(b).

Table 2: Suction cavity's geometric parameters.

Suction cavity	Radius (mm)	15
	Height (mm)	0.2

4.1.3. The Suction Cup with Micropump. Geometric parameters of each element in the micropump are shown in Table 1. The suction cavity's geometric parameters of the suction cup are in Table 2. According to the calculation method derived from the previous section, equivalent electrical network parameters of each element in the micropump suction cup are in Table 3. Equivalent parameters of the piezoelectric actuator and its electrical network model have been given in Section 3.1.2, and the complete equivalent electrical network model of the suction cup with double vibrator micropump is set up in circuit simulation software Multisim 10.0 as shown in Figure 16. In this model, all components have ideal characteristics. A DC power supply with a voltage of 101325V is used to simulate the atmospheric pressure. In the same way, the initial voltage of the equivalent flow capacitance of the vibrating cavity and suction cavity is also 101325V.

4.2. Negative Pressure Response Simulation. According to the above model, the pressure in the micropump suction

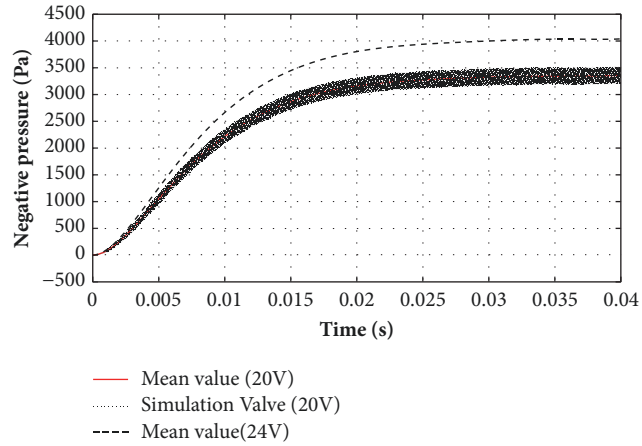

Figure 17: Negative pressure response simulation curve.

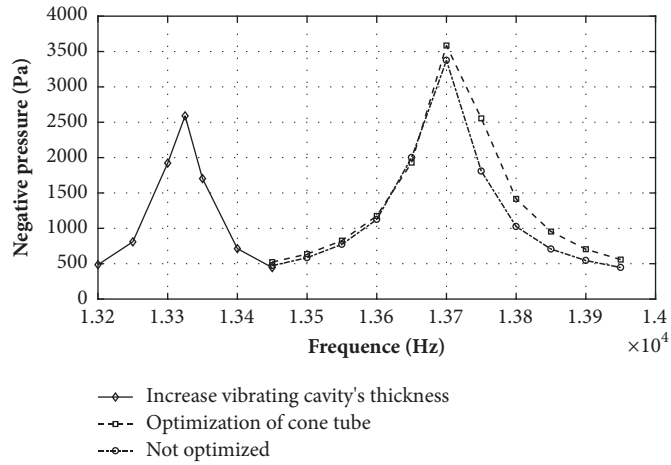

Figure 18: Negative pressure's frequency response curves.

cup's suction cavity is the voltage value in the equivalent capacitance C_s in Figure 16. Figure 17 is the negative pressure response simulation curve. The driving voltage amplitude of piezoelectric actuators is 20V, and its frequency is 13.7 kHz. It can be seen that the negative pressure's instantaneous value (the dotted line in Figure 17) follows the sine law of the driving voltage. The mean value of the negative pressure (the solid line in Figure 17) in the suction cavity also can be obtained by the instantaneous value using data processing software Origin Pro 9.0. The mean negative pressure will eventually increase to a steady-state value, and reach to the maximum back pressure of the micropump under the driving frequency and voltage amplitude. At this time, the micropump cannot continue to extract the air in the suction cavity. The steady-state mean negative pressure of the suction cup is 3.4 kPa, and the response time to the steady-state value is approximately 0.03 s.

In Figure 18, the steady-state mean negative pressure of the suction cup with different geometric size and different actuating frequency is obtained by Multisim 10.0 and Origin Pro 9.0, and the driving voltage amplitude is 20V. In Figure 18, the steady-state mean negative pressure at 13.7 kHz is 3.4 kPa when the suction cup's size is not optimized. When the minimum section width of the cone tube is optimized to 0.21 mm, the steady-state mean negative pressure is 3.6 kPa at the same driving frequency. When the thickness of the vibrating cavity increases to 0.2 mm, the driving frequency corresponding to the maximum steady-state mean negative pressure changes to 13.325 kHz, and the steady-state mean negative pressure decreases to 2.6 kPa. Simulation results show that the driving frequency has great influence on the mean value of steady-state negative pressure, and the driving frequency corresponding to the maximum steady-state negative pressure is close to the natural frequency of the piezoelectric actuator. Simulation results also show that the suction ability of the micropump suction cup can be improved by optimizing the section size of the cone tube and reducing the thickness of the vibrating cavity.

Figure 19 is the relationship between the steady-state mean negative pressure and the driving voltage's amplitude for various micropump suction cups, and the driving frequency is the optimal frequency obtained according to Figure 18. Figure 19 shows that the mean value of the steady-state negative pressure increases linearly with the increase of the

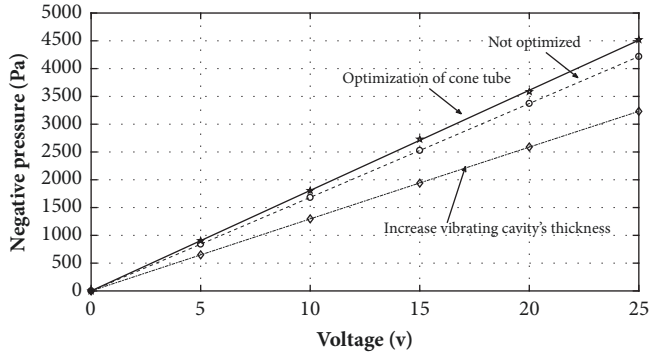

Figure 19: Relationship between the negative pressure and the driving voltage's amplitude.

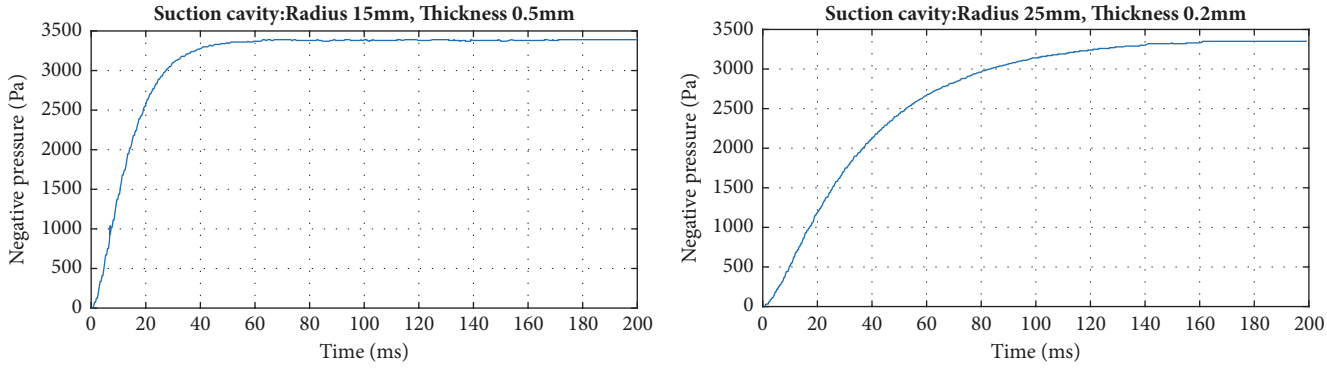

(a) Thickness increase

(b) Radius increase

Figure 20: Influence of suction cavity on negative pressure response.

driving voltage's amplitude. Figure 19 once again illustrates that the suction cup's suction ability can be improved by optimizing the section size of the cone tube and reducing the thickness of the vibrating cavity.

Figure 20 is the negative pressure response curve of suction cup with the original micropump, but the suction cavity's radius and height are changed. Its driving frequency is 13.7 kHz and the driving voltage amplitude is 20 V. Figure 20 is obtained by the circuit simulation software Multisim 10.0 directly. In Figure 20(a), when the radius of the suction cavity is 25 mm and its thickness is 0.2 mm, the negative pressure reaches steady state by 0.175 s; when the radius of the suction cavity is 15 mm and its thickness is 0.5 mm, the negative pressure reaches steady state by 0.075 s (Figure 20(b)). Under different geometric dimensions, the steady-state mean negative pressure is the same and its value is 3.4 kPa. Compared with Figures 17 and 20, it is found that the size of the suction cavity does not affect the steady-state mean negative pressure, because the negative pressure is only related to the air transmission capacity of the micropump, but not to the size of the suction cavity. When the thickness and radius of the suction cavity become larger, the response speed of the negative pressure is slower. The reason is that the micropump has the same ability to extract air, but the amount of air is increased and it should take longer time to extract the air under the same driving condition. Increasing of the suction cup's radius can increase the effective suction area, and its suction force is enhanced. Therefore, we can increase the radius and reduce the thickness of the suction cavity simultaneously to obtain a higher suction force.

5. Conclusions

In order to realize the miniaturization of the suction mechanism for robotics and get a stable negative pressure at the same time, design and simulation of a novel suction cup integrated with a valveless piezoelectric micropump are presented in this paper, and the following conclusions are obtained:

(1) The structure design of the micropump suction cup should be easy to be miniaturized and easy to manufacture, and using the valveless micropump and laminated structure can achieve these.

(2) The systematic optimization design method of the suction cup in this paper is effective. To get a larger volumetric change, theoretical model of the piezoelectric actuator can be used to find the actuator's optimal radius and thickness ratio, and the two ports' equivalent circuit model of piezoelectric actuator can calculate the actuator's resonant frequency.

(3) Finite element analysis results show that the minimum section width, cone angle, and expanding length of the diffuser/nozzle influence its rectification

Table 3: Equivalent electrical network parameters of the micropump suction cup.

Cone tube	Diffuser flow resistance (Jsm^{-6})	$2.8517e+009$
	Diffuser flow inductance (Js^2m^{-6})	$1.1396e+005$
	Nozzle flow resistance (Jsm^{-6})	$3.3530e+009$
	Nozzle flow inductance (Js^2m^{-6})	$1.3399e+005$
Vibrating cavity	Flow Capacitance (m^6J^{-1})	$8.0711e-014$
	Flow inductance (Js^2m^{-6})	1.0439
Suction cavity	Flow Capacitance (m^6J^{-1})	$1.0089e-012$
	Flow inductance (Js^2m^{-6})	0.3340

efficiency. When the other parameters are constant, all of them have the best value.

(4) A modified equivalent circuit modeling method which can improve the efficiency and accuracy of simulation is presented. In this model, static lump parameters are calculated by finite element method to avoid complex theoretical calculation processes. The computing process of the diffuser/nozzle's flow resistance and inductance is also improved by integrating and introducing rectifying efficiency coefficient.

(5) Simulation results based on the equivalent circuit model show that the suction cup can produce a stable negative pressure rapidly. The above-mentioned optimization measures can improve the mean value of the steady-state negative pressure.

There are still some problems in this paper. For example, the backpressure of valveless micropump is lower than that of the valve micropump, which limits the maximum negative pressure, and experimental verification is not carried out. Subsequent studies will be carried out in these areas.

Data Availability

All data used to support the findings of this study are available from the corresponding author upon request.

Conflicts of Interest

The authors declare that there are no conflicts of interest regarding the publication of this paper.

Acknowledgments

This research is partially supported by Shanghai Department of Science and Technology Fund Project for Shanghai Engineering Research Center for Assistive Devices (Grant no. 15DZ2251700).

References

[1] M. Hirai, S. Hirose, and W. Lee, "Gunryu III: Reconfigurable magnetic wall-climbing robot for decommissioning of nuclear reactor," *Advanced Robotics*, vol. 27, no. 14, pp. 1099–1111, 2013.

[2] B. Chu, K. Jung, C.-S. Han, and D. Hong, "A survey of climbing robots: Locomotion and adhesion," *International Journal of Precision Engineering and Manufacturing*, vol. 11, no. 4, pp. 633–647, 2010.

[3] L. Xin, W. Zhong, T. Kagawa, H. Liu, and G. Tao, "Development of a Pneumatic Sucker for Gripping Workpieces with Rough Surface," *IEEE Transactions on Automation Science and Engineering*, vol. 13, no. 2, pp. 639–646, 2016.

[4] S. Nishita and H. Onoe, "Liquid-filled Flexible Micro Suction-Controller Array for Enhanced Robotic Object Manipulation," *Journal of Microelectromechanical Systems*, vol. 26, no. 2, pp. 366–375, 2017.

[5] T. Matsuno, A. Kakogawa, and S. Ma, "Development of a suction cup with a disc spring," in *Proceedings of the 2013 IEEE International Conference on Robotics and Automation, ICRA 2013*, pp. 1362–1367, deu, May 2013.

[6] B. Hu, L. Wang, Y. Zhao, and Z. Fu, "A miniature wall climbing robot with biomechanical suction cups," *Industrial Robot: An International Journal*, vol. 36, no. 6, pp. 551–561, 2009.

[7] H. Feng, W. Dong, and N. Chai, "A bionic micro sucker actuated by IPMC," in *Proceedings of the 2014 IEEE International Conference on Orange Technologies (ICOT)*, pp. 223–226, Xi'an, China, September 2014.

[8] T. Takahashi, K. Nagato, M. Suzuki, and S. Aoyagi, "Flexible vacuum gripper with autonomous switchable valves," in *Proceedings of the 2013 IEEE International Conference on Robotics and Automation, ICRA 2013*, pp. 364–369, deu, May 2013.

[9] A. Olsson, G. Stemme, and E. Stemme, "First valve-less diffuser gas pump," in *Proceedings of the 1997 10th Annual International Workshop on Micro Electro Mechanical Systems, MEMS*, pp. 108–113, January 1997.

[10] M. Richter, R. Linnemann, and P. Woias, "Robust design of gas and liquid micropumps," *Sensors and Actuators A: Physical*, vol. 68, no. 1, pp. 480–486, 1998.

[11] T. Gerlach, "Pumping gases by a silicon micro pump with dynamic passive valves," in *Proceedings of the 1997 International Conference on Solid-State Sensors and Actuators. Part 1 (of 2)*, pp. 357–360, June 1997.

[12] T. Gerlach and H. Wurmus, "Working principle and performance of the dynamic micropump," *"Sensors and Actuators, A: Physical"*, vol. 50, no. 1-2, pp. 135–140, 1995.

[13] J. Wang, K. C. Aw, A. McDaid, and R. N. Sharma, "An Efficiency improved diffuser with extended sidewall for application in valveless micropump," *Heat and Mass Transfer*, vol. 52, no. 4, pp. 913–923, 2016.

[14] T.-Q. Truong and N.-T. Nguyen, "A polymeric piezoelectric micropump based on lamination technology," *Journal of Micromechanics and Microengineering*, vol. 14, no. 4, pp. 632–638, 2004.

[15] Q. Cui, C. Liu, and X. F. Zha, "Simulation and optimization of a piezoelectric micropump for medical applications," *The International Journal of Advanced Manufacturing Technology*, vol. 36, no. 5-6, pp. 516–524, 2008.

[16] C. Mo, R. Wright, W. S. Slaughter, and W. W. Clark, "Behaviour of a unimorph circular piezoelectric actuator," *Smart Materials and Structures*, vol. 15, no. 4, pp. 1094–1102, 2006.

[17] S. A. N. Prasad, Q. Gallas, S. Horowitz et al., "Analytical electroacoustic model of a piezoelectric composite circular plate," *AIAA Journal*, vol. 44, no. 10, pp. 2311–2318, 2006.

[18] Y.-C. Hsu and N.-B. Le, "Inertial effects on flow rate spectrum of diffuser micropumps," *Biomedical Microdevices*, vol. 10, no. 5, pp. 681–692, 2008.

[19] A. Olsson, G. Stemme, and E. Stemme, "Numerical and experimental studies of flat-walled diffuser elements for valve-less micropumps," *Sensors and Actuators A: Physical*, vol. 84, no. 1, pp. 165–175, 2000.

[20] E. Morganti, I. Fuduli, A. Montefusco, M. Petasecca, and G. U. Pignatel, "SPICE modelling and design optimization of micropumps," *International Journal of Environmental Analytical Chemistry*, vol. 85, no. 9-11, pp. 687–698, 2005.

[21] M. Aumeerally and R. Sitte, "Layered fluid model and flow simulation for microchannels using electrical networks," *Simulation Modelling Practice and Theory*, vol. 14, no. 1, pp. 82–94, 2006.